ISBN: 978-628-95207-4-3. ISSN: 2414-6390. Digital Object Identifier: https://dx.doi.org/10.18687/LACCEI2023.1.1.1279

# Cinematic Design and Force Analysis of a SCARA Robot with Pneumatic Actuators

Daniel Mencia, Mechatronic Engineer[1], Michael Ramos, Mechatronic Engineer [2], Favell Nuñez, Master in Robotics [3], and Jose Luis Ordoñez-Avila, Master in Industrial Engineering[4]
[1,2,3,4] FI, Universidad Tecnológica Centroamericana (UNITEC), Honduras, daniel.lmencia@unitec.edu, m.ramos@unitec.edu eduardo.nunez@unitec.edu.hn, jlordonez@unitec.edu

***Abstract*– The use of pneumatics applied to industry is greatly favored by its great availability and for being a non-polluting fluid, thus having a potential to replace other systems in the industry. In the field of industrial robotics, a robotic arm with pneumatic servomotors is rarely designed, as there are few studies about it. This technology being a closed loop repetitive control system with feedback makes feasible its implementation for processes in the industry. Since there are few pneumatic industrial robots, this study seeks to design a prototype with an analysis for the precise control of the positions and reduce the nonlinear randomness of the pneumatic system, through the resolution of the kinematics, which will provide necessary information on the mechanical adjustments in the pneumatic servomotors for a required application as well as the interpretation of transmission simulations. This study provides a manufacturing model of a fully pneumatic and functional robotic prototype, opening the field for future research on pneumatic control applied to industrial robotics.***

***Keywords*-- rotary actuator; pneumatics; cinematic model; robotic arm; transmission force.**

## I. Introduction

At present, articulated arms are one of the most used robotic systems by the industry worldwide. A robotic arm is an electromechanical device formed by joints and links, driven by an electric, pneumatic, or hydraulic mechanism. These sources are used to perform the movement, guided by sensors that provide information to the micro controller to manipulate objects and perform different operations. The operations depend on the application, which perform repetitive tasks with great precision and accuracy, can be classified into angular robots, cylindrical, polar, Cartesian and SCARAs [1].

Due to the great demand in the industry to automate their processes to improve efficiency, the field of robotics is growing and having the need to find a variety of alternatives for the design and manufacture different typed of robots. Although pneumatics is widely used in the industry, the use of pneumatic systems as full motion drive for robots is still very uncommon, so it is necessary to perform studies on the modeling of manipulators composed by pneumatic servo positions to facilitate the use of this technology that has the potential to replace the other systems in many applications [2].

The disadvantage of pneumatic systems is their non-linearity so it is necessary to have a wide knowledge of the system to reduce the randomness in the dynamics of the movement, that is affected by the pressure inside the cylinder chambers, variation in friction and the flow of air through the valves so it is usually preferred to use other linear systems in which there is more precision in controlling the movement but pneumatic actuators have many advantages over other systems such as cleanliness, low cost of implementation, high power to weight ratio, easy maintenance, safety, explosion-proof, long service life and as pneumatic systems are driven by compressed air they have high availability and reduce environmental pollution [3].

Any application in which a robotic arm is used requires the design of a trajectory, in which the behavior of the robot is planned according to the work area to perform its task reaching a suitable position and orientation for the end effector [4]. Most of the time the structure of the robotic arms used is in series due to the lower complexity in kinematics and the advantages of a larger working space compared to the closed structure [5] due to close structures such as [6]. The inverse kinematics is the opposite seeks to find the positions and orientation of the links or body of the robot with respect to a reference that is the end effector [7].

The Denavit-Hartenberg (DH) convention is commonly used in the kinematic analysis based on parameters. These parameters are given to each joint to build the table, from which it will derive a homogeneous transformation matrix. The DH transforms are composed of pure rotation and pure translation matrices, which can be represented as follows: Ti− i 1 = Rxi−1(αi−1), Txi−1(αi−1), Tzi(di), Rzi(θi). Often for simulation and verification of the direct and inverse kinematics, tools like MATLAB Robotic Toolbox are used [8,9].

The opposite of direct kinematics is inverse kinematics, which describes the mapping of joint coordinates to the known variables of the end-effector position. Trajectory control is the most important part of kinematics and is the basis for planning the robot's movements. Solving kinematic problems with inverse kinematics is much more difficult and complete than direct kinematics except for robots with parallel kinematics, so before using it, certain criteria must be considered: the ability to solve as the amount of DOF (Degrees of Fredom) and that unlike the direct in the inverse there are multiple solutions due to its non-linearity [10].

Extensive studies have been made about inverse kinematic, the current methods for the solution of the inverse kinematic problem are algebraic and geometric analysis. The configuration of each position in the inverse kinematics has two conditions of analysis: elbow down and elbow up, highlighting that the geometric analysis is more illustrative due to the use of graphs that serve to make the study less complicated, analyzing

**Digital Object Identifier:** (only for full papers, inserted by LACCEI).
**ISSN, ISBN:** (to be inserted by LACCEI).
**DO NOT REMOVE**

them with geometry methods using Pythagoras and trigonometric theorems to find the angles of both links [11].

SCARA robots are mechatronic devices that use rotary and linear actuators for the positioning of their end-effector, they have a movement that resembles the human arm simulating the shoulder, elbow, and wrist. Therefore, precision, smoothness of movement and efficiency, are being used on a recurring Basisen automation of processes such as assembly, packaging, pick and place [12].

This state of the art has been shown to demonstrate the applications of SCARA robots. These applications are in all industries although none were found that use pneumatic actuators. These actuators are very inexpensive and common in industry. This study focuses on the fabrication of a fully pneumatic SCARA 4DOF robot using a kinematic model for motion control. The objective is to expand the knowledge on the use of pneumatic actuator technology, making use of kinematics for orientation and angular positions as required in the application together with a motion simulation for force transmission analysis.

## II. Materials and Methods

Mechatronic products require a different approach than conventional ones as it integrates several scientific disciplines (mechanical, electrical and information). It was used as research frame of reference the V-methodology of Vasić & Lazarević, which follows a set of guidelines for a transversal analysis separating each of the systems, sub systems and parts to perform an transversal integration of the parts, sub systems and systems, with the objective of helping the product developer to reduce costs and time while delivering an efficient and verified product [13].

For the first stage of the manufacture of the 4DOF pneumatic arm, a CAD design was made to make a prototype and to establish the requirements of the dimensions of the links, stability of the joints and to perform laboratory tests with simulations of movement and stress of the parts to be manufactured. As well as simulations to determine the most appropriate type of power transmission for the robot: direct drive power transmission or power transmission with synchronous belts.

The next stage in the V methodology as shown in the illustration in Fig. 1, is analysis and development of the mechatronic systems design.

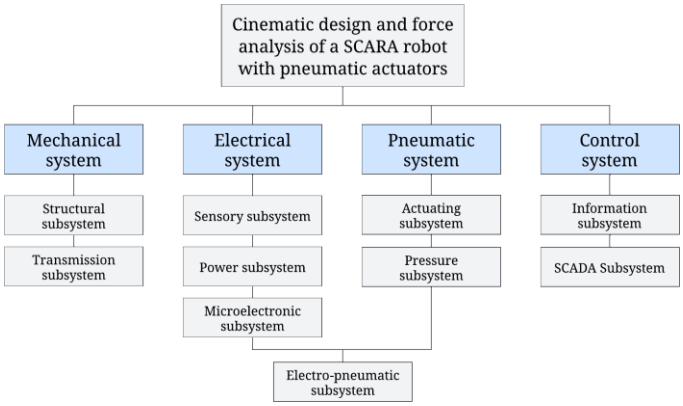


Fig. 1 V method structure.

### *A. Mechanical System*

The mechanical system will determine the structural stability of the robot under internal or external loads, performing the movement which is given by the transmission of force that will be exerted by the type of mechanical energy applied on the joints. Therefore, the mechanical system is composed of different subsystems. The structural subsystem analyzes all the part of the rigid elements of the robot, ball bearing elements and type of joints for the articulation. The pneumatic subsystem being a type of mechanical energy will analyze the drive and fluid pressures delivered to the actuators of the robot. Finally, transmission subsystem is the relationship that exists between the actuator and the links for the transmission of force.

### *B. Electrical System*

The electronic system will deal with the design of a command circuit for the control of the robot by means of the integration of different subsystems. The sensory subsystem necessary to provide information converted into digital signals to indicate the end of the trajectory and identify the positioning in the robot's workspace. The power subsystem responsible for powering all electronic components of the robotic arm. The drive subsystem using an electro-pneumatic system to control the direction of the fluid direction understandable through the microcontroller.

### *C. Control System*

The control system will provide the information for the orientation and position of the robot in space for a given application. It is divided into the following subsystems: information subsystem in charge of managing the digital signals of the sensors and actuators established by the microcontroller ,and the SCADA subsystem operator/machine interface that will allow to supervise the operation of the robotic arm.

### *D. Parts definition*

The structure of the manipulator was 3d printed. PLA+ was chosen for the fabrication of the links of the SCARA robot's structural subsystem due to its greater resistance to impact and

elongation at break. The transmission subsystem was made from the results of the force analysis, using HDT synchronous belts and toothed pulleys. For the pneumatic subsystem, the following pneumatic servo systems SMC-MSQB20A, Festo DSR-16-180-P, DSR-12-180-P and ADVU-16-70-P-A were used. For the sensing subsystem, SMC-D-A93 inductive sensors and OMRON V-156-1C25 limit sensors were used. For the microelectronics subsystem, SIEMENS PLC-1200 microcontroller was used to manage the inputs and outputs of the control circuit. For the information system, the kinematic behavior of the robot must be known, and its programming will be based on DH convention analysis for direct kinematics and trigonometric analysis for direct kinematics resolution. Finally, a SIEMENS HMI will be used for the SCADA system.

*E. System integration*

The last stage in the V methodology, is the integration of all the parts, subsystems, and systems in that sequence in order to get the efficient fabrication of the prototype of the pneumatic SCARA robot 4DOF.

## III. Mechanism Simulations

As part of the research, we had to make an important decision which involved deciding between a direct drive power transmission or power transmission with synchronous belts. For this reason, a motion analysis was made to determine which method of transmitting power was more efficient. Both designs were identical aside from the way of transmitting power and were tested using the same positions.

Based on the above parameters the CAD software has given us the following results which have been represented in graphs, joining the results of each motor with transmission and with direct coupling.

Figures 3 shows the power consumption graphs which allow us to compare the energy consumed in watts of these motors. In the graphs we can see how the actuator with direct drive transmission consumes more energy than the transmission system with timing belts.

Figure 4 shows the torque which allow us to compare the amount of torque produce by each motor. On the left we can appreciate a higher torque produced from the direct drive transmission to move the part on of the robotic arm which translates on more power consumption.

Figure 5 shows the total kinetic energy of the tip of the SCARA robot. This energy is measured at the top of the end effector.

This robot configuration has an effective working area of 370mm radius when the base actuator is at 0 or 180 degrees as shown in Figure 6. It then extends behind the base with a radius of 197.93mm due to the second rotary actuator. This is only possible when the first actuator is at either 0 or 180 degrees. The part where the end effector would be mounted also has its respective rotary and linear actuator.

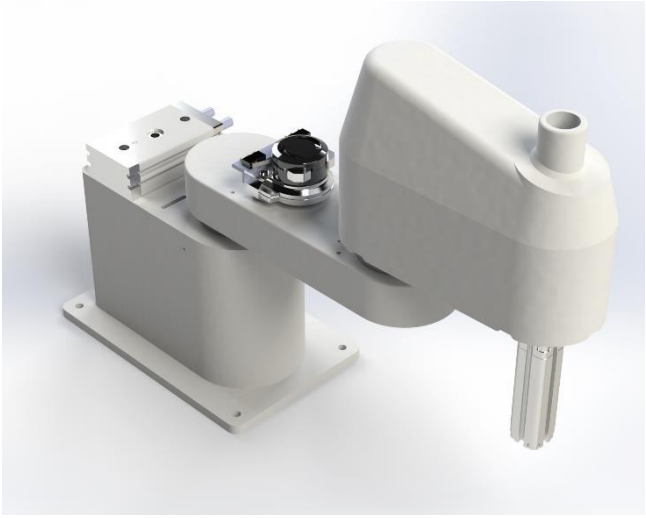

Fig. 2 Isometric view of SCARA prototype.

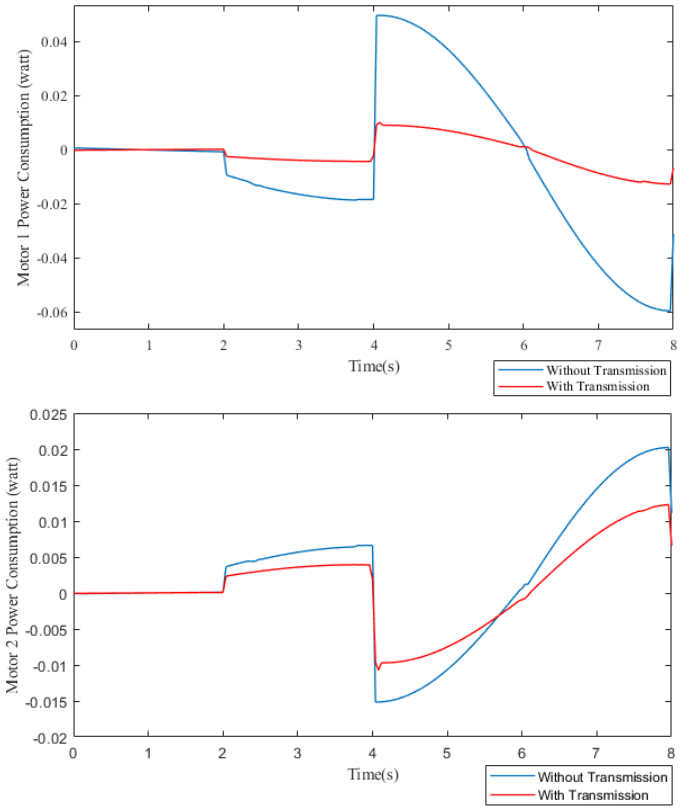


Fig. 3 Power consumption of motor 1 and 2.

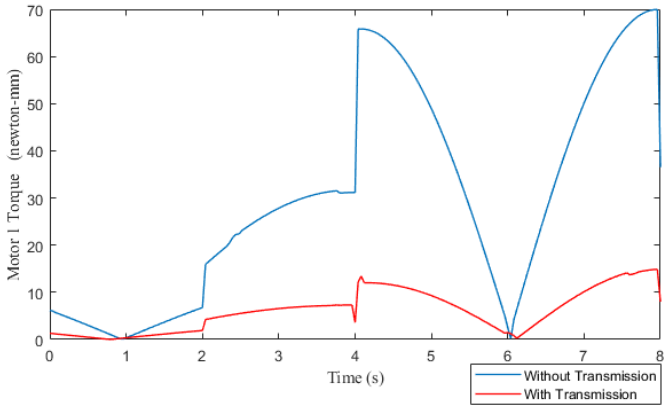


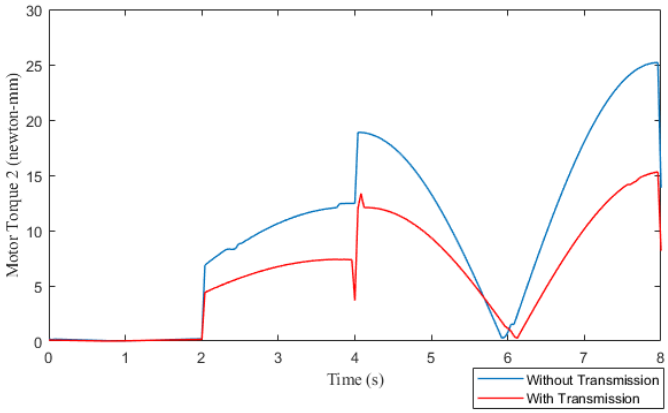


Fig. 4 Torque of motor 1 and 2.

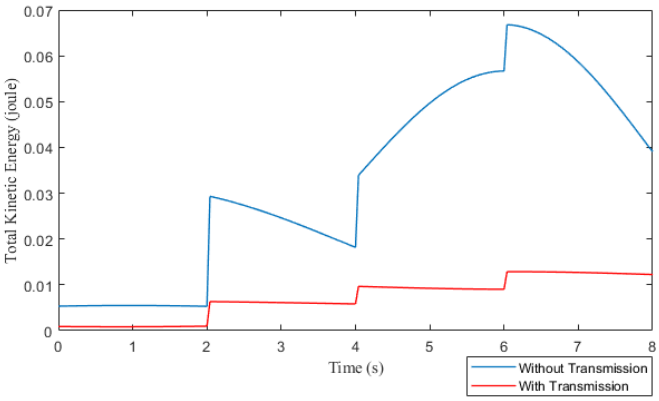


Fig. 5 Kinetic energy.

## IV. CINEMATIC MODEL

### A. *Mechanic System*

A fundamental part of this project also consisted of creating the pieces in a physical way. That is why additive printing was chosen as a fundamental part for the creation of the links. The base has a height of 168mm, a width of 117mm and a length of 228.5mm. The distance between centers is 121.5mm. The center link has a height of 44mm, a width of 100mm and a length of 303mm. The distance between centers is 121.5mm. The last link has a height of 8.5mm, a maximum width of 105mm, and a length of 250mm. The total height is 286mm, length is 588mm and width is 117mm. Pla+ has been used as a material due to its tensile strength, density and ease of printing properties. Previous research has shown that the tensile mechanical properties of PLA are greater than ABS if printed at 0° or 90° degrees which is the case [14]. Also an infill of more than 70% was used to avoid mechanical stress [15]

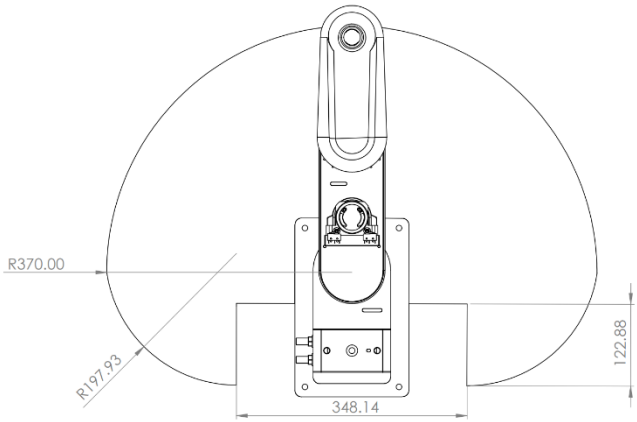


Fig. 6 Work area of pneumatic SCARA 4 DOF.

### B. *Electronic System*

The electronics system is responsible for integrating the microelectronics, power electronics and sensory part of the robot into a control circuit for the drive and control of the robot for a given process. Because this arm was to work in conjunction with a Siemens PLC it was chosen to use a 24 V DC power supply. This served to power everything from the PLC and sensors to the solenoid valves. For the solenoid valves we used a bank of SMC sy3140-5ldz solenoid valves, all 8 of which were needed for the required movements. For each of the joints different actuators were used, for the rotary joint of the base with the first link (N°1 GDL) the SMC-MSQB20A actuator was used, for the rotary joint of the first link with the second link (N°2 GDL) the DSR-16-180-P actuator was used, for the final rotary and linear joint movements (N°3 and N°4 GDL) the DSR-12-180-P and ADVU-16-70-P-A actuators were used respectively.

### C. *Control System based on kinematics.*

For the resolution of the direct kinematics, use was made of the DH convention, the Denavit-Hartenberg parameters were compiled from a series of data obtained from the robot body, its links and joints as shown in Figure 7 as [16].

The result of the homogeneous matrices are obtained by the sequence of the joints and the parameters in the DH table as shown in the equation.

$$T_{i-1}^{i} = \boldsymbol{R_{xi-1}}(\alpha_{i-1}), \boldsymbol{T_{xi-1}}(a_{i-1}), \boldsymbol{T_{zi}}(d_i), \boldsymbol{R_{zi}}(\theta_i)$$

$$T_4^0 = T_1^0, T_2^1, T_3^2, T_4^3 \quad (1)$$

In the first joint matrix there are two parameters represented with one homogeneous matrix each, a rotational matrix in the axis Z $R_{zi}(\theta_i)$ , one translation in the X-axis $T_{xi-1}(a_{i-1})$ and a last translation in the Z-axis $T_{zi}(d_i)$ resulting in (2) and (3).

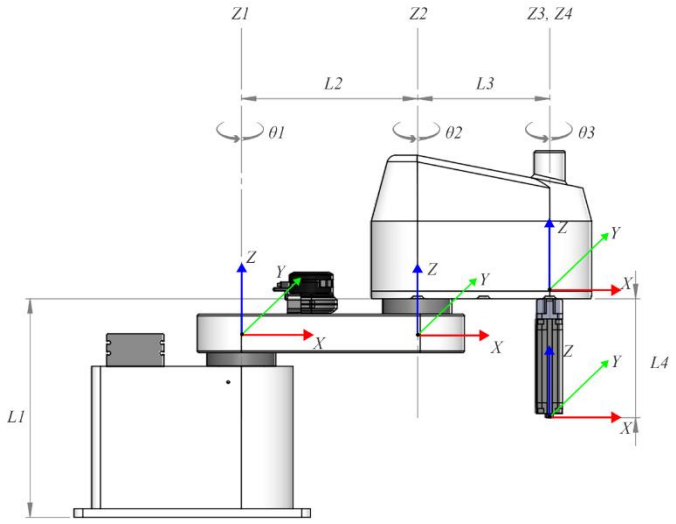


| Unión | $\theta_i$ | $d_i$ | $a_i$ | $\alpha_i$ | Rango |
|---|---|---|---|---|---|
| 1 | $\theta_1$ | 250 | 200 | 0 | −90° 90° |
| 2 | $\theta_2$ | 0 | 150 | 0 | −90° 90° |
| 3 | $\theta_3$ | 0 | 0 | 0 | −90° 90° |
| 4 | 0 | $-d_4-135.5$ | 0 | 0 | 135.5 183.5 |

Fig. 7 Work area of pneumatic SCARA 4 DOF

$$T_{\theta_1} = \begin{bmatrix} \cos\theta_1 & -sen\ \theta_1 & 0 & 0 \\ sen\ \theta_1 & \cos\theta_1 & 0 & 0 \\ 0 & 0 & 1 & 0 \\ 0 & 0 & 0 & 1 \end{bmatrix} \times T_b$$

$$= \begin{bmatrix} 1 & 0 & 0 & 0 \\ 0 & 1 & 0 & 0 \\ 0 & 0 & 1 & d_i \\ 0 & 0 & 0 & 1 \end{bmatrix} \times T_a$$

$$= \begin{bmatrix} 1 & 0 & 0 & a_i \\ 0 & 1 & 0 & 0 \\ 0 & 0 & 1 & 0 \\ 0 & 0 & 0 & 1 \end{bmatrix} (2)$$

$$T_1^0 = \begin{bmatrix} \cos\theta_1 & -sen\ \theta_1 & 0 & L_2\cos\theta_1 \\ sen\ \theta_1 & \cos\theta_1 & 0 & L_2\cos\theta_1 \\ 0 & 0 & 1 & L_1 \\ 0 & 0 & 0 & 1 \end{bmatrix} (3)$$

In the second joint matrix there are two parameters represented with one homogeneous matrix each, a rotational matrix in the axis Z $R_{zi}(\theta_i)$ one translation in the X-axis $T_{xi-1}(a_{i-1})$ and a last translation in the Z-axis $T_{zi}(d_i)$ resulting in (4) and (5).

$$T_{\theta_2} = \begin{bmatrix} \cos\theta_2 & -sen\ \theta_2 & 0 & 0 \\ sen\ \theta_2 & \cos\theta_2 & 0 & 0 \\ 0 & 0 & 1 & 0 \\ 0 & 0 & 0 & 1 \end{bmatrix} \times T_{a_2}$$

$$= \begin{bmatrix} 1 & 0 & 0 & a_2 \\ 0 & 1 & 0 & 0 \\ 0 & 0 & 1 & 0 \\ 0 & 0 & 0 & 1 \end{bmatrix} (4)$$

$$T_2^1 = \begin{bmatrix} \cos\theta_2 & -sen\ \theta_2 & 0 & L_3\cos\theta_2 \\ sen\ \theta_2 & \cos\theta_2 & 0 & L_3 sen\ \theta_2 \\ 0 & 0 & 1 & 0 \\ 0 & 0 & 0 & 1 \end{bmatrix} (5)$$

In the third joint matrix there are two parameters represented with one homogeneous matrix each, a rotational matrix in the axis Z $R_{zi}(\theta_i)$ resulting in (6) and (7).

$$T_{\theta_3} = T_3^2 = \begin{bmatrix} \cos\theta_3 & -sen\ \theta_3 & 0 & 0 \\ sen\ \theta_3 & \cos\theta_3 & 0 & 0 \\ 0 & 0 & 1 & 0 \\ 0 & 0 & 0 & 1 \end{bmatrix} (6)$$

$$T_4^3 = \begin{bmatrix} 1 & 0 & 0 & 0 \\ 0 & 1 & 0 & 0 \\ 0 & 0 & 1 & -d_4 - L_4 \\ 0 & 0 & 0 & 1 \end{bmatrix} (7)$$

As a result of the trajectory of the SCARA robotic arm represented in joint matrices in equation (1), which when multiplied we obtain the resulting matrix of the DH parameters resulting in equation (8).

$$T_4^0 =$$

$$\begin{bmatrix} c(\theta_1+\theta_2+\theta_3) & -s(\theta_1+\theta_2+\theta_3) & 0 & L_3\,c(\theta_1+\theta_2)+L_2\,c(\theta_1) \\ s(\theta_1+\theta_2+\theta_3) & c(\theta_1+\theta_2+\theta_3) & 0 & L_3\,s(\theta_1+\theta_2)+L_2\,s(\theta_1) \\ 0 & 0 & 1 & L_1-L_4-d_4 \\ 0 & 0 & 0 & 1 \end{bmatrix}$$

The DH parameters of the SCARA 4GDL pneumatic robot were simulated again in Matlab software, but this time using Peter Corke's Toolbox Robotics, in which a training animation of the robot was performed with the DH parameters, giving the angular coordinates $\theta_1 = 0°$ y $\theta_2 = 0°$ as shown in Figure 8.

$$[x, y, z, r, p, y] = [306.066, 106.066, 114.5, 45, 0, 0]$$

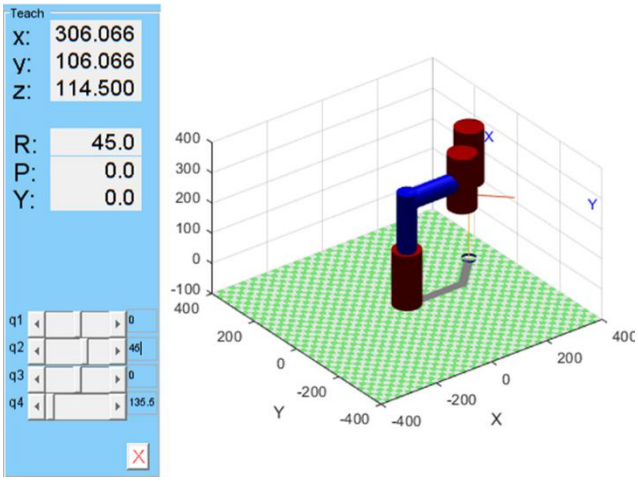


. Fig. 8 Work area of pneumatic SCARA 4 DOF.

The resolution of the inverse kinematics can be solved by different methods and can have different solutions being a nonlinear system. For the resolution of the inverse kinematics of the SCARA 4GDL pneumatic robot the geometric method was used, analyzing it from a top view considering that the SCARA robots are planar robotic arms in which a relationship is found between the angles of the revolution movements and the distance of the links as can be seen Figure 9.

The geometric analysis was performed from a fixed reference point $P$ and $P_x$, $P_y$, $P_z$ variables in which it depends on the already known coordinates of the end effector to find the position and orientation of the joints.

$$P = \begin{bmatrix} P_x \\ P_y \\ P_z \end{bmatrix}$$

In order to find $P_z$ the ratio of the links $L_1$ and $L_4$ the variable distance of the prismatic joint, in (9) was added.

$$\boldsymbol{P_z} = L_1 - L_4 - d_4 \quad (9).$$

In the geometrical analysis of the SCARA robot diagram, we can find a relationship between the angles $\alpha$ and $\theta_2$ expressed in (10).

$$180 = \alpha + \theta_2;\ \alpha = 180 - \theta_2 \quad (10)$$

For the resolution of the obtuse triangle of blue and yellow color was analyzed, in which the law of cosines was applied (11) and clearing for cosine (12) in which the hypotenuse R in the diagram and in the formula is already known by applying the Pythagorean theorem (13), in which substituting in the equation is expressed as follows according to the values of links and the variable coordinate system (14).

$$c^2 = a^2 + b^2 - 2bc\ \cos\alpha \ (11)$$

$$-\cos\alpha = \frac{c^2 - a^2 - b^2}{2ab} \ (12)$$

$$c = \sqrt{{P_x}^2 + {P_y}^2} \ (13)$$

$$-\cos\alpha = \frac{{P_x}^2 + {P_y}^2 - {L_2}^2 - {L_3}^2}{2L_2L_3} \ (14)$$

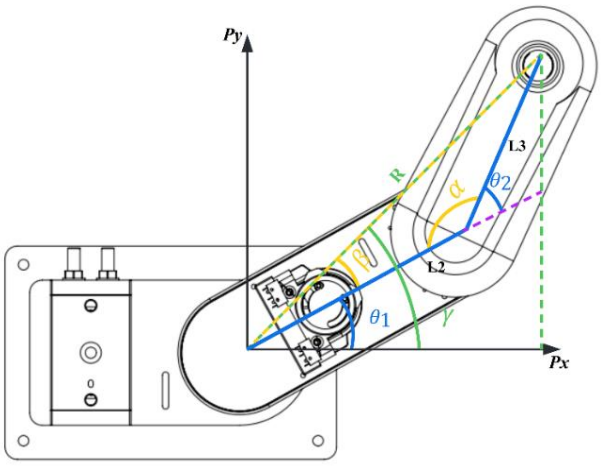


Fig. 9 Work area of pneumatic SCARA 4 DOF.

We substitute the known value of the equation (14) in the equation and applying the trigonometric identity (15) we can leave the positive equation (16).

$$\cos(\pi - \alpha) = -\cos\alpha$$

$$\therefore \cos(180 - \theta_2) = \frac{{P_x}^2 + {P_y}^2 - {L_2}^2 - {L_3}^2}{2L_2L_3} \ (15)$$

$$\cos\theta_2 = \frac{{P_x}^2 + {P_y}^2 - {L_2}^2 - {L_3}^2}{2L_2L_3} (16)$$

In order to leave the equations as a tangent function, we use the law of cosines, being able to substitute the equation (16) in (18) giving as a result the equation for of the following form (19).

$$\theta_2 = \tan^{-1}\left(\frac{\sqrt{1 - \cos^2\theta_2}}{\cos\theta_2}\right) \ (18)$$

$$\boldsymbol{\theta_2} = \tan^{-1}\left(\frac{\sqrt{1-\left(\frac{P_x{}^2 + P_y{}^2 - L_2{}^2 - L_3{}^2}{2L_2L_3}\right)^2}}{\frac{P_x{}^2 + P_y{}^2 - L_2{}^2 - L_3{}^2}{2L_2L_3}}\right) (19)$$

The expression of $\theta_1$ is found in the ratio of the angles $\gamma$ and $\beta$ in the right triangle formed by $P_x$ and $P_y$ (20), coordinates of the position and orientation of the end-effector in which gamma can be obtained by tangent and beta $\beta$ can be obtained by extending the obtuse triangle with trigonometric functions as a function of the values of the links and substituting (16) and (17) in equation (22), resulting in the equation for $\theta_1$ the following equation (23).

$$\theta_1 = \gamma - \beta \ (20)$$

$$\theta_1 = \tan^{-1}\left(\frac{P_y}{P_x}\right) - \beta \ (21)$$

$$\theta_1 = \tan^{-1}\left(\frac{P_y}{P_x}\right) - \tan^{-1}\left(\frac{L_3 \sin\theta_2}{L_2 + L_3\cos\theta_2}\right) (22)$$

$$\boldsymbol{\theta_1} = \tan^{-1}\left(\frac{P_y}{P_x}\right) - \tan^{-1}\left(\frac{L_3\sqrt{1-\frac{P_x{}^2 - P_y{}^2 - L_2{}^2 + L_3{}^2}{2L_2L_3}}}{L_2 + L_3\frac{P_x{}^2 - P_y{}^2 - L_2{}^2 + L_3{}^2}{2L_2L_3}}\right) (23)$$

For the verification of the inverse kinematics, we use the direct kinematics obtained in the Matlab in which the position and orientation of the end effector in the vector plane is already known. When $\theta_1 = 90°$ and $\theta_2 = 45°$ the kinematic position of the direct is given by the vectors (24).

$$(x, y, z, r, p, y)(-106.0660, 306.0660, 114.5, 135, 0, 0) \quad (24)$$

Substituting the values of the links and the vectors of the position and orientation in the inverse kinematics, the following results were obtained.

$$\boldsymbol{P_z} = 200 - 135.5 - 0 = 114.5$$

$$\boldsymbol{\theta_1} = \tan^{-1}\left(\frac{306.0660}{-106.0660}\right) - \tan^{-1}\left(\frac{106.0660}{306.0660}\right) = 90°$$

$$\boldsymbol{\theta_2} = \tan^{-1}\left(\frac{0.7071070172}{0.7071065452}\right) = 45°$$

$$\boldsymbol{\alpha} = 180 - 45 = 135°$$

## V. Dynamic Concepts

The configuration of the SCARA Robot is an RRRP, having the three rotational joints in a plane and the prismatic joint perpendicular to it. Given this, we can decompose the robot in a plane manipulator, having a 3R, and separately the prismatic joint with a translational motion perpendicular to the plane. The 3R plane configuration allows us to apply the Newton-Euler method to derive the dynamic model for this part. The force equations for the fourth joint will be calculated separately following a pneumatic cylinder analysis.

The outward recursion computes the velocities and accelerations in each link. This procedure follows a set of six steps, calculating for each link:

1. Angular velocity of the link. $\dot{\theta}$ represents the joint velocity.
2. Angular acceleration of the link. $\ddot{\theta}$ represents the joint acceleration.
3. Linear acceleration of link at frame origin. *L* is the length of the link.
4. Linear acceleration at the centroid of the link. *c* is the distance of the centroid in the x axis from the origin´s link frame.
5. Resultant force acting on the centroid of the link. *m* is the mass of the link.
6. Resultant moment acting around the centroid of the link. *I* represents the moment of inertia at the center of mass.

Link 1:

$$\begin{aligned}
&1.\ \omega_1 = \dot{\theta}_1 \\
&2.\ \dot{w}_1 = \ddot{\theta}_1 \\
&3.\ {}^1\dot{V}_2 = L_1\begin{bmatrix} -w_1^2 \\ \dot{\omega}_1 \end{bmatrix} \\
&4.\ {}^1a_1 = \begin{bmatrix} -c_1w_1^2 \\ c_1\dot{w}_2 \end{bmatrix} \\
&5.\ {}^1F_1 = m_1{}^1a_1 \\
&6.\ N_1 = I_1\dot{\omega}_1
\end{aligned} \quad (25)$$

Link 2:

$$\begin{aligned}
&1.\ \omega_2 = \omega_1 + \dot{\theta}_2 \\
&2.\ \dot{w}_2 = \dot{w}_1 + \ddot{\theta}_2 \\
&3.\ {}^2\dot{V}_1 = {}^2R_1 \cdot {}^1\dot{V}_1 = \begin{bmatrix} C_2 & -S_2 \\ S_2 & C_2 \end{bmatrix} \cdot {}^1\dot{V}_1 \\
&{}^2\dot{V}_2 = {}^2\dot{V}_1 + L_2\begin{bmatrix} -\omega_2^2 \\ \dot{\omega}_2 \end{bmatrix} \\
&4.\ {}^2a_2 = {}^2\dot{v}_1 + \begin{bmatrix} -c_2\omega_2^2 \\ c_2\dot{w}_2 \end{bmatrix} \\
&5.\ {}^2F_2 = m_2{}^2a_2 \\
&6.\ N_2 = I_2\dot{\omega}_2
\end{aligned} \quad (26)$$

Link 3:

$$
\begin{aligned}
&1.\ W_3 = W_2 + \dot{\theta}_3 \\
&2.\ {}_3 = \dot{w}_2 + \ddot{\theta}_3 \\
&3.\ {}^3\dot{V}_2 = {}^3R_2 \cdot {}^2\dot{V}_2 = \begin{bmatrix} C_3 & -S_3 \\ S_3 & C_3 \end{bmatrix} \cdot {}^2\dot{V}_2 \\
&\quad {}^3\dot{V}_3 = {}^3\dot{V}_2 + L_3 \begin{bmatrix} -\omega_2^2 \\ \dot{\omega}_2 \end{bmatrix} = {}^3\dot{V}_2 \\
&4.\ {}^3a_3 = {}^3\dot{V}_2 \\
&5.{}^3F_3 = m_3{}^3a_3 \\
&6.\ N_3 = I_3\dot{\omega}_3
\end{aligned}
\tag{27}
$$

Link 4:

We analyse the dynamic modelof the fourth joint , Fig 10, separately from the other three rotational articulations. This mechanism uses as pneumatic cylinder as a prismatic joint. Therefore, the model relates the force of the cylinder with the air pressure and its exerted motion.

h = Travel Distance
Fp = Cylinder retracting force
p = Pressure
m = External mass
d1 = Cylinder diameter
d2 = Stem diameter

$$F_p = P\left(\frac{d_1^2 - d_2^2}{4}\right)\pi - m \cdot g$$

$$F_p = m \cdot g$$

$$a = \frac{F_p}{m}$$

$$V_f^2 = V_o^2 + 2 \cdot a \cdot h$$

$$V_f^2 = 2 \cdot a \cdot h$$

$$V_f^2 = \pm\sqrt{2 \cdot a \cdot h}$$

$$a = \frac{V_f}{t}; t = \frac{V_f}{a}$$

(26)

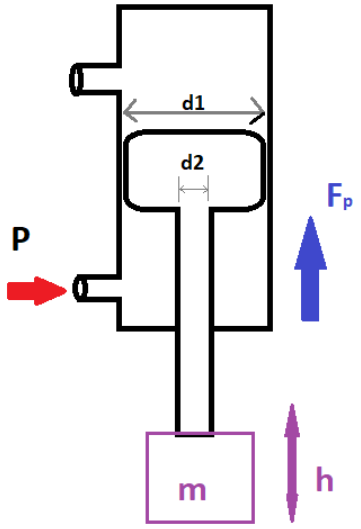


Fig. 10 Dynamics of the fourth link.

## V. Control and Electrical System

The control system was programmed in TIA PORTAL using the ladder language in which simple movements were performed due to the characteristics of pneumatics as shown in Figure 11. Two main movements were programmed, one with all actuators to the right and another with all actuators to the left. This was to check that all actuators were operating as expected. We also programmed an HMI (Fig. 12) with 3 basic buttons, two of them being a movement to the right and one to the left. The last button is the one that contracts the piston in manual mode, autonomously an inductive sensor was programmed for which the robotic arm when detecting that an object is found performs a Pick and Place operation autonomously according to the sequence of the signal from the sensors at the end of the stroke in the PLC inputs and triggering the output signal to activate the solenoid of the solenoid valves and thus move the plunger to one direction or another of the actuators or joints.

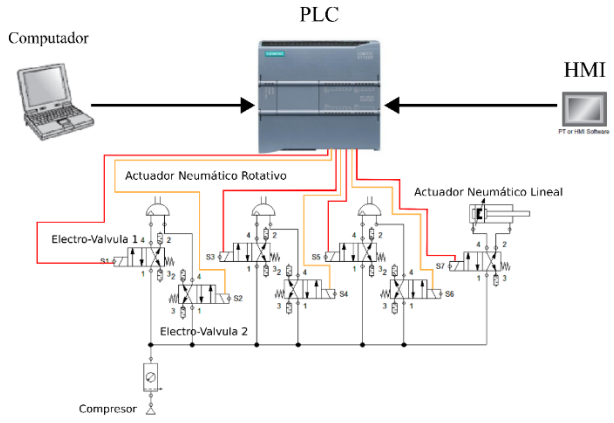


Fig. 11 Architecture of the robot controller.

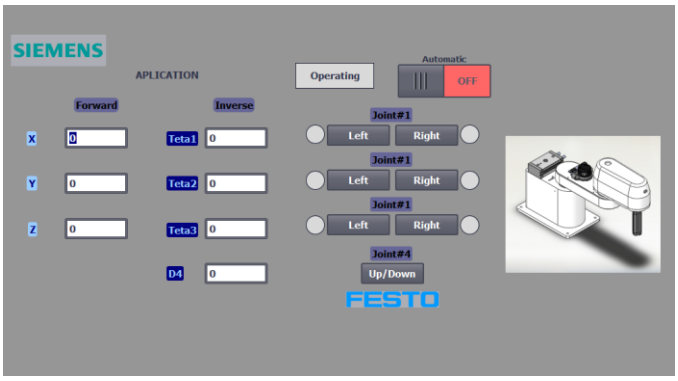

Fig. 12 HMI application.

## VI. Conclusion

The fabrication of a fully pneumatic 4DOF SCARA Robot was carried out, in which the analysis of the mechanical, electrical and control systems along with their subsystems and parts for its development is addressed. Equations were used for the kinematic and dynamic model that was validated with simulations in Matlab and experimentally in the physical prototype. Mechanical adjustments of the angular limits in the actuators for the displacement obtained in the kinematics were made, based on a given application. This gave excellent results in the tests for the angular positions. Pneumatics can be perfectly applied to the use of industrial robotics for processes of a given task of fixed initial and final stroke at high speeds.

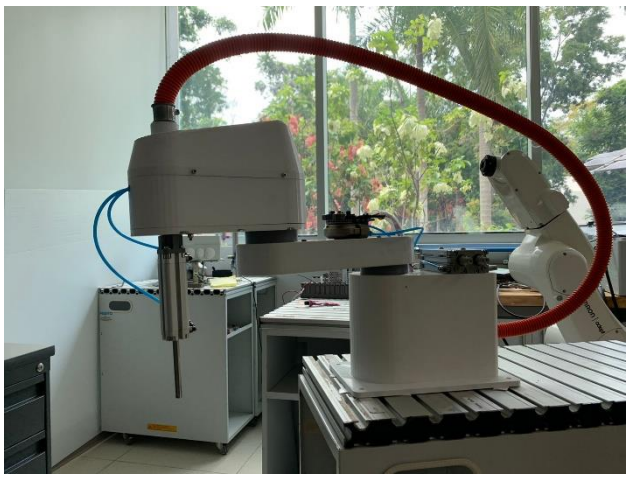
Fig. 13 Work area of pneumatic SCARA 4 DOF.

## References

[1] Jahnavi, K.; Sivraj, P. Teaching and learning robotic arm model. In Proceedings of the 2017 International Conference on Intelligent Computing, Instrumentation and Control Technologies (ICICICT), 2017, pp. 1570–1575. https://doi.org/10.1109/ICICICT1.2017.8342804.

[2] Schluter, M.; Perondi, E. Mathematical Modeling with Friction of a SCARA Robot Driven by Pneumatic Semi-rotary Actuators. IEEE Latin America Transactions 2020, 18, 1066–1076. Conference Name: IEEE Latin America Transactions, https://doi.org/10.1109/TLA.2020.9099684.

[3] Saravanakumar, D.; Mohan, B.; Muthuramalingam, T. A review on recent research trends in servo pneumatic positioning systems. Precision Engineering 2017, 49, 481–492. https://doi.org/10.1016/j.precisioneng.2017.01.014.

[4] Coman, G.C.; Serban, C.; Ivan, A.M.; Nicolescu, A.F. Virtual prototyping, physical structure development and PC control of a double arm (five link) SCARA robot. IOP Conference Series: Materials Science and Engineering 2019, 591, 012075. https://doi.org/10.1088/1757-899X/591/1/012075.

[5] Shen, H.; Liu, Y.; Wu, H.; Hu, C.; Wang, S. Forward and Inverse Kinematics for a Novel Double Scara Robot. IOP Conference Series: Earth and Environmental Science 2018, 170, 042088. https://doi.org/10.1088/1755-1315/170/4/042088.

[6] Saraf, M.; Agarwal, A.; Chaudhary, A.; Ganthale, A. Kinematic Modelling and Motion Mapping of Robotic Arms. Journal of Physics: Conference Series 2021, 1969, 012002. https://doi.org/10.1088/1742-6596/1969/1/012002.

[7] Luan, Y.; Xu, W.; Li, J.; Zhou, D.; Wang, H.; Ji, H. Kinematics Modeling and Simulation of a 4-DOF Manipulator. In Proceedings of the 2017 International Conference on Computer Systems, Electronics and Control (ICCSEC), 2017, pp. 302–305. https://doi.org/10.1109/ICCSEC.2017.8446769.

[8] J. L. Ordoñez-Avila, M. Cardona, D. A. Aguilar, M. Ordoñez and C. L. Garzón-Castro, "A Novel Monitoring System for Contagious Diseases of Patients using a Parallel Planar Robot," 2022 IEEE International Conference on Machine Learning and Applied Network Technologies (ICMLANT), Soyapango, El Salvador, 2022, pp. 1-6, doi: 10.1109/ICMLANT56191.2022.9996485.

[9] Lee, J.W.; Park, G.T.; Shin, J.S.; Woo, J.W. Industrial robot calibration method using denavit — Hatenberg parameters. In Proceedings of the 2017 17th International Conference on Control, Automation and Systems (ICCAS), 2017, pp. 1834–1837. https://doi.org/10.23919/ICCAS.2017.8204265.

[10] Parvathi, S.; Selvi, S.T. Design and fabrication of a 4 Degree of Freedom (DOF) robot arm for coconut harvesting. In Proceedings of the 2017 International Conference on Intelligent Computing and Control (I2C2), 2017, pp. 1–5. https://doi.org/10.1109/I2C2.2017.8321925.

[11] Yao, C.; Voronin, S.S. The Kinematic Analysis of the SCARA on MATLAB. In Proceedings of the 2018 International Conference on Industrial Engineering, Applications and Manufacturing (ICIEAM), 2018, pp. 1–6. https://doi.org/10.1109/ICIEAM.2018.8728847.

[12] Suri, S.; Jain, A.; Verma, N.; Prasertpoj, N. SCARA Industrial Automation Robot. In Proceedings of the 2018 International Conference on Power Energy, Environment and Intelligent Control (PEEIC), 2018, pp. 173–177. https://doi.org/10.1109/PEEIC. 2018.8665440.

[13] Vasi´c, V.; Lazarevi´c, M. Standard Industrial Guideline for Mechatronic Product Design. FME Transactions 2008, 36.

[14] Jaisingh Sheoran, A.; Kumar, H. Fused Deposition modeling process parameters optimization and effect on mechanical properties and part quality: Review and reflection on present research. 21, 1659–1672. https://doi.org/10.1016/j.matpr.2019.11.296.

[15] J. L. O. Avila, M. E. Perdomo, M. Y. R. Bejarano, y J. L. O. Fernández, «Mechanical Displacement for 3D Printers' Parts Using FEM as Inverse Engineering Method in Honduras», J. Phys. Conf. Ser., vol. 1877, n.o 1, p. 012013, abr. 2021, doi: 10.1088/1742-6596/1877/1/012013.

[16] Nguyen, H.X.; Nguyen, H.C.; Mai, N.A.; Nguyen, H.T.; Tran, D.X.; Dang, L.B.; Pham, H.M.; Dinh, L.N. Performance evaluation of an inverse kinematic based control system of a humanoid robot arm using MS Kinect. In Proceedings of the 2017 IEEE International Conference on Robotics and Biomimetics (ROBIO), 2017, pp. 469–474. https://doi.org/10.1109/ROBIO.2017.8324461.M. Young, *The Technical Writer's Handbook*, Mill Valley, CA: University Science, 1989.